# Ligand Binding Alters the Backbone Mobility of Intestinal Fatty Acid-Binding Protein as Monitored by $^{15}$N NMR Relaxation and $^{1}$H Exchange†

Michael E. Hodsdon and David P. Cistola*

*Department of Biochemistry & Molecular Biophysics, Washington University School of Medicine, St. Louis, Missouri 63110*

*Received August 13, 1996; Revised Manuscript Received November 26, 1996*⊗

ABSTRACT: The backbone dynamics of the liganded (holo) and unliganded (apo) forms of *Escherichia coli*-derived rat intestinal fatty acid-binding protein (I-FABP) have been characterized and compared using amide $^{15}$N relaxation and $^{1}$H exchange NMR measurements. The amide $^{1}$H/$^{15}$N resonances for apo and holo I-FABP were assigned at 25 °C, and gradient- and sensitivity-enhanced 2D experiments were employed to measure $^{15}$N $T_1$, $T_2$, and {$^{1}$H}$^{15}$N NOE values and relative $^{1}$H saturation transfer rates. The $^{15}$N relaxation parameters were analyzed using five different representations of the spectral density function based on the Lipari and Szabo formalism. A majority of the residues in both apo and holo I-FABP were characterized by relatively slow hydrogen exchange rates, high generalized order parameters, and no conformational exchange terms. However, residues V26−N35, S53−R56, and A73−T76 of apo I-FABP were characterized by rapid hydrogen exchange, low order parameters, and significant conformational exchange. These residues are clustered in a single region of the protein where variability and apparent disorder were previously observed in the chemical shift analyses and in the NOE-derived NMR structures of apo I-FABP. The increased mobility and discrete disorder in the backbone of the apo protein may permit the entry of ligand into the binding cavity. We postulate that the bound fatty acid participates in a series of long-range cooperative interactions that cap and stabilize the C-terminal half of helix II and lead to an ordering of the portal region. This ligand-modulated order−disorder transition has implications for the role of I-FABP in cellular fatty acid transport and targeting.

Intestinal fatty acid-binding protein (I-FABP)[1] is a predominately $\beta$-sheet protein that binds a single molecule of long chain fatty acid. It is abundantly expressed in small intestinal enterocytes and thought to function in the transport and trafficking of fatty acids absorbed from the lumen. However, the precise function of I-FABP is not well-understood, and the molecular mechanisms by which it regulates fatty acid transfer within the cell have not been defined. In particular, it is not clear how fatty acid enters and exits the protein and how the protein delivers fatty acid to target sites in the cell.

We recently determined the NMR solution structures of the liganded and unliganded forms of I-FABP in order to learn more about its conformational properties in solution (Hodsdon *et al.*, 1995, 1996; Hodsdon & Cistola, 1997). The holo and apo structures were determined using essentially identical 3D (three-dimensional) triple-resonance NMR protocols, and each structure was based on over 3300 conformational restraints. Unlike the holo form, the ensemble of NMR structures of apo I-FABP exhibited variability in a discrete region of the protein backbone (Hodsdon & Cistola, 1997). The apparent disorder was most pronounced in residues 29−36 and 54−57, corresponding to the distal half of α-helix II, the linker between helix II and $\beta$-strand B, and the turn between $\beta$-strands C and D (Figure 1). The disorder in apo I-FABP was also shown by differences in the $^{1}$H/$^{13}$C consensus chemical shift indices and the positions of missing amide proton resonances relative to the holo protein. This backbone disorder, which was not a feature of the 1.2 Å X-ray crystal structure (Scapin *et al.*, 1992),[2] was characterized by a destabilization of long-range interactions between helix II and the C−D turn and a fraying of the C-terminal half of helix II. This disordered region of the protein backbone appears to consititute a flexible, dynamic portal that permits the entry of fatty acid. We proposed that the binding of fatty acid leads to an ordering of helix II by stabilizing a series of long-range cooperative interactions resembling a C-terminal helix capping box (Hodsdon & Cistola, 1997).

In the present study, we have characterized the dynamic properties of I-FABP in order to further evaluate the apparent backbone disorder observed in the NMR structure of the apo

† This work was supported by grants from the National Science Foundation (MCB-9205665 to D.P.C.), the American Digestive Health Foundation, and institutional startup funds. The Unity-500 spectrometer was supported in part by the Markey Center for Research in the Molecular Biology of Disease at Washington University. D.P.C. gratefully acknowledges a Johnson & Johnson/Merck Research Scholar Award from the American Digestive Health Foundation.

* To whom correspondence should be addressed: Campus Box 8231, Washington University School of Medicine, 660 South Euclid Ave., St. Louis, MO 63110-1093. Phone: 314-362-4382. Fax: 314-362-4153. E-mail: cistola@cosine.wustl.edu.

⊗ Abstract published in *Advance ACS Abstracts,* February 1, 1997.

[1] Abbreviations: iLBPs, intracellular lipid-binding proteins; I-FABP, intestinal fatty acid-binding protein; H-FABP, heart/muscle fatty acid-binding protein; A-LBP, adipocyte lipid-binding protein; I-LBP, ideal lipid-binding protein; NOE, nuclear Overhauser effect; HSQC, heteronuclear single-quantum correlation spectroscopy; $T_1$, longitudinal relaxation time constant; $T_2$, transverse relaxation time constant; $\tau_m$, overall correlation time; $\tau_e$, effective correlation time for internal motions; $S^2$, generalized order parameter; $R_{ex}$, conformational exchange term; 2D, two-dimensional.

[2] In the 1.2 Å X-ray crystal structure of apo I-FABP, helix II is well-defined. In addition, the main chain temperature factors for residues 25−36 and 54−57 are low and not significantly different from the rest of the protein backbone (1IFC; Brookhaven PDB). There are no obvious or specific intermolecular contacts in the crystalline lattice that might lead to an ordering of these residues.

S0006-2960(96)02018-1 CCC: $14.00 

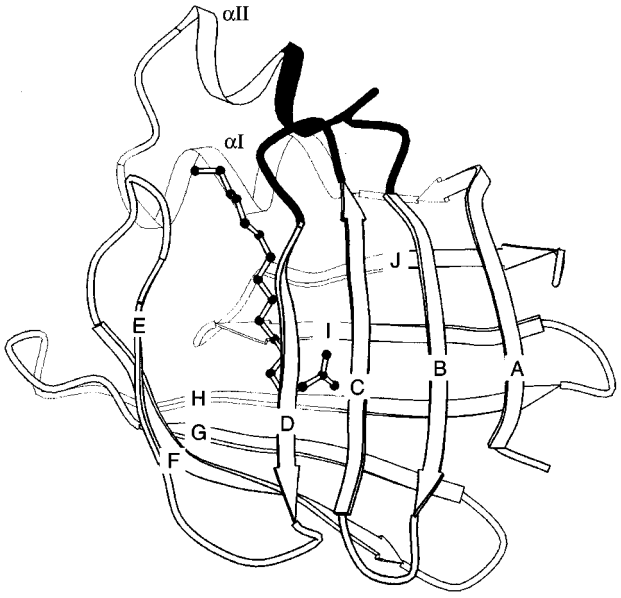


FIGURE 1: Ribbon diagram of the NMR solution structure of rat I-FABP complexed with palmitate (Hodsdon *et al*., 1996). The bound fatty acid is shown in ball-and-stick format. The region shaded black exhibited apparent backbone disorder in the NMR solution structure of the *unliganded* form of the protein, as shown in Figure 7 (Hodsdon & Cistola, 1997).

protein. Amide $^1$H exchange and $^{15}$N relaxation rates in the presence and absence of bound fatty acid were monitored and compared using $^1$H/$^{15}$N NMR and a uniformly $^{15}$N-enriched protein. Residues in the vicinity of helix II and the C−D and E−F turns were more mobile than other parts of the molecule, especially in the apo protein. The increased mobility was shown by higher rates of amide $^1$H exchange, lower order parameters, and sizable conformational exchange terms. In contrast, the remainder of the protein backbone was characterized by slow hydrogen exchange, high order parameters, and vanishing conformational exchange terms. The dynamic results reinforce the conclusions drawn from a comparision of the chemical shifts and the NOE-derived structures of apo and holo I-FABP and indicate that the local variability in the ensemble of apo NMR structures represents increased backbone mobility in a specific region of the protein. The results provide insights into a possible mechanism by which I-FABP and other lipid-binding proteins may regulate fatty acid transfer and targeting in the cell.

## MATERIALS AND METHODS

*Sample Preparation.* Uniformly $^{15}$N-enriched I-FABP was biosynthesized in *Escherichia coli* MG-1655 using a strategy designed to achieve an optimal balance between cell growth and isotope utilization. Bacteria harboring the pMON5840-I-FABP plasmid were initially grown overnight at 37 °C in a non-isotope-enriched and nutrient-supplemented M9 medium similar to that of Li *et al.* (1987) containing trace metals and thiamine but lacking casamino acids and yeast extract. This culture was harvested by centrifugation, and a portion of the cell pellet was used to seed a New Brunswick Bioflo-III high-density fermentor equipped with a 1.25 L vessel containing an otherwise identical medium, but initially lacking glucose and ammonium chloride. Logarithmic growth was supported by periodic additions of nutrients, including a total of 26 g of unenriched glucose and 6 g of [99.5%-$^{15}$N]ammonium chloride (Isotec lot OU0978). During growth, the presence of glucose in the medium was monitored by the use of Diastix reagent strips (Miles, Inc., Elkhart, IN), the type used by diabetic subjects to monitor urinary glucose, and maintained at a level of 0.1−0.2% (w/v). Protein expression, under control of the recA promoter, was induced with nalidixic acid at a cell density of ∼13 $OD_{600}$ units. The cells continued to grow for ∼3 h to an OD of 26, at which point the cells were harvested and stored at −70 °C for further processing.

The protocols for protein purification and delipidation have been detailed elsewhere (Lowe *et al.*, 1987; Jakoby *et al.*, 1993). A portion of the delipidated, concentrated protein sample containing 10% $D_2O$ was used to prepare a stoichiometric complex with palmitate as described by Cistola *et al.* (1989). The apo/holo homogeneity of the samples was verified by 2D $^1$H/$^{15}$N HSQC NMR. Most of the apo and holo I-FABP resonances are not superimposable (Figure 2), and samples containing mixtures of apo and holo protein contain two distinct sets of resonances. Therefore, the possibilities of incomplete delipidation or incomplete complex formation could be ruled out in this manner. The final protein concentration in the NMR samples was 2 mM with a buffer composition of 20 mM potassium phosphate, 50 mM potassium chloride, and 0.05% sodium azide at pH 7.2.

*NMR Spectroscopy*. All NMR spectra were accumulated with a Varian Unity-500 spectrometer equipped with a Performa II pulsed field gradient amplifier and a Nalorac 5 mm ITG-500-5 triple-resonance probe with an actively shielded *z*-axis gradient coil. Quadrature detection in the indirectly detected dimension was achieved using hypercomplex data collection. With the exception of the temperature series described below, all spectra were acquired at 25 °C. Gradient- and sensitivity-enhanced $^1$H−$^{15}$N HSQC spectra were aquired using the pulse sequence of Kay and co-workers (Zhang *et al*., 1994; Muhandiram & Kay, 1994) with acquisition parameters summarized in the legend of Figure 2. In addition, a single 3D $^{15}$N TOCSY-HMQC spectrum was collected on apo I-FABP at 25 °C using the pulse sequence, aquisition, and processing parameters detailed in Hodsdon *et al*. (1995).

The pulse sequences used to determine $^{15}$N $T_1$, $T_2$, and $\{^1H\}^{15}N$ NOE values were those detailed in Figure 10 of Farrow *et al*. (1994). These experiments employ minimal saturation of the water resonance and thus minimize any potential complications from hydrogen exchange. Spectra were collected at 25 °C using acquisition parameters identical to those described in Figure 2 for the HSQC spectra and similar to those of Farrow *et al.* (1994), except as noted below. The spectra used to measure $T_1$, $T_2$, and $\{^1H\}^{15}N$ NOE values were acquired in duplicate. The peak intensities in the $T_1$ and $T_2$ experiments relax in a monoexponential fashion during the relaxation delay, $T$, in such a way that the length of the postacquisition delay prior to the beginning of the pulse sequence affects only the sensitivity and not the extracted relaxation times (Sklenar *et al.*, 1987). Backbone amide $^{15}$N $T_1$ values were measured from two series of seven spectra with the following relaxation delay times: $T$ = 28.1, 112.2, 224.4, 336.6, 448.9, 617.2, and 785.5 ms, and $T$ = 28.1, 56.1, 112.2, 196.4, 280.5, 392.8, and 561.1 ms. Amide $^{15}$N $T_2$ values were obtained similarly: $T$ = 16.0, 32.1, 48.1, 80.2, 112.2, 144.3, and 176.4 ms, and $T$ = 16.0, 32.1, 48.1, 64.1, 80.2, 112.2, and 160.3 ms. In order to estimate the signal-to-noise and reproducibility of peak

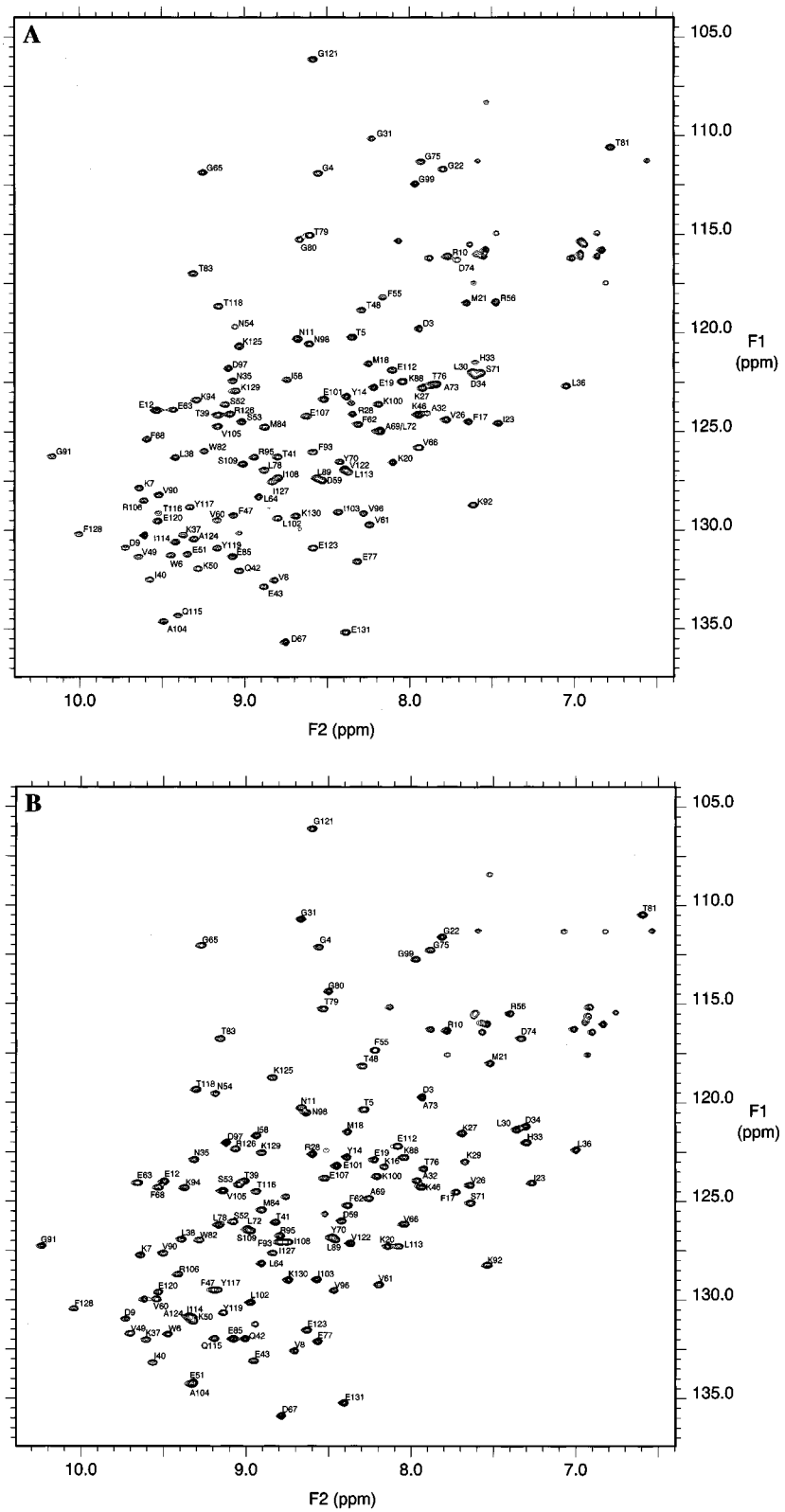


FIGURE 2: Gradient- and sensitivity-enhanced 2D $^1H-^{15}N$ HSQC spectra of uniformly $^{15}N$-enriched I-FABP in the absence (A) and presence (B) of bound palmitate. Backbone amide correlations are labeled according to the assignments described in the text and are available as Supporting Information. The spectra were collected using the pulse sequence described in the text with a 3.0 and 6.5 kHz spectral width and 256 and 512 complex points in the $F_1(^{15}N)$ and $F_2(^1H)$ frequency dimensions, respectively. Each FID consisted of eight averaged, successive scans separated by a 1.0 s relaxation delay; the total experimental time was 81 min. A delay value of 2.3 ms ($<1/4J_{NH}$) was employed during the INEPT subsequences; a 2.0 ms low-power, rectangular pulse was used to selectively excite the water resonance and return its magnetization to an equilibrium state, and WALTZ-16 was used for broad band decoupling during acquisition. The unlabeled resonances in the upper right quadrant of each spectrum represent side chain $NH_2$ correlations in Asn and Gln residues.

intensities, spectra at the longest relaxation delays were collected in triplicate. Steady-state $\{^1H\}^{15}N$ NOE values were obtained by recording spectra with (NOE experiment) and without (NONOE experiment) the use of $^1H$ saturation applied during the delay between successive transients. In the NONOE experiment, a relaxation delay of 5 s was

employed between transients, while the NOE experiment employed a 2 s delay plus 3 s of proton presaturation achieved with the use of 120° $^1$H pulses applied every 5 ms (Markley *et al.*, 1971).

*Data Processing and Analysis*. Initial processing of the time-domain spectra was performed on a Sun SPARC-2 workstation using VNMR v. 4.2 (Varian Associates). The spectra were zero-filled to 512 × 1024 real points and pseudo-echo weighted along the $F_1$ dimension with a −5 Hz line broadening and a Gaussian factor of 0.056. For spectral analysis, the processed and phased frequency-domain spectra were imported into NMR Compass v. 2.5 (Molecular Simulations, Inc.) running on a Silicon Graphics INDY/R4400 workstation. Peak intensities in the spectra were estimated from their peak heights obtained using the automated peak-picking and refinement routine contained within the software. An analysis of selected relaxation decay curves revealed essentially identical decay results when intensities were measured according to peak heights or volumes. However, measurement of peak volumes generally produced increased scatter and uncertainty in the resulting decay curves, possibly resulting from the difficulty of determining the appropriate spectral baseline for volume measurements. Hence, peak heights were considered more precise and reliable indicators of relative intensity.

For both the $T_1$ and $T_2$ spectra, peak intensities from the two time courses were normalized according to the first delay time and combined for fitting. Relaxation times were determined by fitting to a two-parameter function of the form

$$I(t) = I_0 \exp(-t/T_{1,2}) \quad (1)$$

where $I(t)$ is the intensity after a delay of time $t$ and $I_0$ is the initial intensity. Optimum values for the parameters were determined by the method of least-squares fitting performed using a modified Powell minimization algorithm in the software package SCIENTIST (MicroMath Scientific Software, Salt Lake City, UT). The goodness of fit of the experimental data to the monoexponential decay function was assessed in SCIENTIST using 95% confidence limits calculated by a rigorous search[3] of the error function. For purposes of input to the spectral density function analysis software described below, the standard errors of the $T_1$ and $T_2$ relaxation times were estimated as $^1/_2$ of the 95% confidence limits.[4]

Steady-state {$^1$H}$^{15}$N NOE values were determined from the ratio of the peak intensities with and without $^1$H saturation and averaged for the duplicate spectra. The standard deviation of the NOE was estimated from an analysis of the background noise in these spectra as detailed in Farrow *et al.* (1994). Standard deviations calculated in this fashion were found to be comparable to the difference between the values calculated from the separate spectra; the larger of the two was utilized as the estimate of the standard error for input to the spectral density calculations.

The $T_1$ and $T_2$ relaxation times and the NOE of the backbone amide $^{15}$N are influenced by the strength of the dipolar interaction with its attached proton and, to a lesser extent, the chemical shift anisotropy of the $^{15}$N nucleus (Abragam, 1961). In solution, the motions of the N−H bond axis are responsible for the strength of the dipolar interaction and, hence, the relaxation of the amide $^{15}$N. These motions are characterized by a set of spectral density functions, $J(\omega)$, at five distinct frequencies. The spectral densities are proportional to the amplitude of the fluctuating magnetic fields at specific frequencies and can be directly related to the three $^{15}$N relaxation parameters (Abragam, 1961; Farrow *et al.*, 1994).

$$T_1^{-1} = d^2[J(\omega_H-\omega_N) + 3J(\omega_N) + 6J(\omega_H+\omega_N)] + c^2J(\omega_N) \quad (2)$$

$$T_2^{-2} = 0.5d^2[4J(0) + J(\omega_H-\omega_N) + 3J(\omega_N) + 6J(\omega_H) + 6J(\omega_H+\omega_N)] + (1/6)c^2[3J(\omega_N) + 4J(0)] \quad (3)$$

$$\mathrm{NOE} = 1 + (\gamma_H/\gamma_N)d^2[6J(\omega_H+\omega_N) - J(\omega_H-\omega_N)]T_1 \quad (4)$$

The constants $d^2$ and $c^2$ are defined as

$$d^2 = 0.1\gamma_H^2\gamma_N^2h^2/(4\pi^2)\langle 1/r_{NH}^3\rangle^2 \quad (5)$$

$$c^2 = (2/15)\gamma_N^2H_0^2(\sigma_{||} - \sigma_\perp)^2 \quad (6)$$

where $\gamma_H$ and $\gamma_N$ are the gyromagnetic ratios of the $^1$H and $^{15}$N nuclei, respectively, $\omega_H$ and $\omega_N$ are their Larmor precessional frequencies, respectively, $r_{NH}$ is their internuclear distance (1.02 Å), and $H_0$ is the magnetic field strength. The parallel and perpendicular components of the axially symmetrical $^{15}$N chemical shift tensor are represented by $\sigma_{||}$ and $\sigma_\perp$, respectively. The assumption of an axially symmetric chemical shift tensor has been shown to be valid for protein−backbone amides and has a value of −160 ppm for $\sigma_{||} - \sigma_\perp$ (Hiyama *et al.*, 1988).

In order to obtain useful information about protein dynamics from the $^{15}$N relaxation parameters, a functional form for the spectral density is required. Three separate descriptions of the spectral density are often used, each expressing a different dependence on the molecular motions responsible for relaxation. The first of these is known as the model-free formalism (Lipari & Szabo, 1982a,b) and employs a minimum of parameters to describe the overall tumbling of the macromolecule and its internal motions with the expression

$$J(\omega) = \frac{S^2\tau_m}{1 + \omega^2\tau_m^2} + \frac{(1 - S^2)\tau}{(1 + \omega^2\tau^2)} \quad (7)$$

The dynamics of each backbone amide are characterized by a time-correlation function factorizable into two independent components: the overall tumbling of the macromolecule and

[3] Statistical calculations were performed in SCIENTIST using a rigorous modeling of the support plane confidence ranges (Box *et al.*, 1978) with the underlying assumption of correlated fitting parameters and nonlinearity of the error function near the minimum.

[4] The spectral density analysis algorithm of Farrow *et al.* (1994) required estimates of the standard deviation of the measured relaxation parameters. The standard deviation is defined for a Gaussian or normal population distribution at the 67% confidence limit, and the 95% limit is equal to 1.96 times the standard deviation. However, 95% confidence limits were determined in SCIENTIST without the assumption of a normal distribution. For the relaxation analysis, the standard deviations were estimated by dividing the 95% confidence limits by 1.96. Because the 95% confidence limits determined in the more rigorous support-plane analysis are at least twice those determined using a normal distribution, the estimates of the standard deviations were larger than if a simpler statistical model had been used.

the internal motions of the N−H bond vector. The correlation function for the overall tumbling is assumed to be isotropic and monoexponential with the time constant $\tau_m$. The internal motions are approximated by a correlation function of the form

$$C_1(t) = S^2 + (1 - S^2)e^{-t/\tau_e} \quad (8)$$

where $S^2$ is known as the generalized order parameter, a model-independent measure of the degree of spatial restriction of the motion bounded by $0 \leq S^2 \leq 1$. If the internal motion is isotropic, $S^2$ vanishes; whereas, when the amide is completely restricted in its motion, $S^2$ equals unity. The effective correlation time resulting from internal motions is $\tau_e$, where

$$1/\tau = 1/\tau_m + 1/\tau_e \quad (9)$$

The second model of the spectral density function considered invokes the use of an additional term, $R_{ex}$, to account for the contribution to the transverse relaxation rate from processes other than the dipole−dipole interaction and chemical shift anisotropy. In most cases, these contributions are the result of conformational exchange averaging. The additional term is included by a modification of the transverse relaxation rate:

$$1/T_2 = 1/T_{2(DD)} + 1/T_{2(CSA)} = R_{ex} \quad (10)$$

where the DD and the CSA subscripts refer to the contributions of the dipole−dipole interaction and the chemical shift anisotropy to the relaxation, respectively. Whereas the generalized order parameter and internal correlation time are sensitive to motions faster than the overall correlation time ($\tau_e$ is generally in the range of nanoseconds to picoseconds), chemical exchange processes contributing to the $R_{ex}$ term occur on a time scale several orders of magnitude slower (milliseconds to microseconds). Nicholson *et al.* (1995) have shown that for a single exchange process involving two equally populated states $R_{ex}$ is insignificant unless the exchange time constant $t_{ex}$ (=2/$k$), where $k$ is the rate constant for the exchange, is greater than $10^{-6}$ s.

Finally, an extended form of the model-free formalism has been developed (Clore *et al.*, 1990a,b) to describe internal motions that take place on two distinct time scales, differing by at least 1 order of magnitude, and affecting all three NMR relaxation parameters: $T_1$, $T_2$, and NOE. The generalized order parameter then becomes a product of the individual fast and slow time scale order parameters,

$$S^2 = S_f^2 S_s^2 \quad (11)$$

Assuming that the correlation time describing the faster of the two time scales, $\tau_f$, is sufficiently small so as to make a neglibible contribution to the relaxation, the extended spectral density can be described

$$J(\omega) = \frac{S^2 t_m}{1 + \omega^2 \tau_m^2} + \frac{(S_f^2 - S^2)\tau}{1 + \omega^2 \tau^2} \quad (12)$$

where the effective correlation time for slow internal motions, $\tau_s$, is included in the relationship

$$1/\tau = 1/\tau_m + 1/\tau_s \quad (13)$$

In order to determine the most appropriate form of the spectral density for modeling the $^{15}$N NMR relaxation of each residue, the protocol described by Farrow *et al.* (1994) was followed. Each spectral density function was fit to the relaxation parameters using a nonlinear least-squares optimization and Monte Carlo error analysis according to the equation

$$\chi^2 = \frac{(T_{1c} - T_{1e})^2}{\sigma_{T_1}^2} + \frac{(T_{2c} - T_{2e})^2}{\sigma_{T_2}^2} + \frac{(T_{NOE_c} - T_{NOE_e})^2}{\sigma_{NOE}^2} \quad (14)$$

where $T_{1c}$, $T_{2c}$, and $NOE_c$ are the relaxation parameters calculated from the spectral density function and $\sigma_{T_1}$, $\sigma_{T_2}$, and $\sigma_{NOE}$ are the estimates of the standard error (described above) of the experimentally determined parameters: $T_{1e}$, $T_{2e}$, and $NOE_e$. Overall, five representations of the spectral density function were considered. The first two were based simply on the single time scale model-free formalism given in eq 7 with fitting of $S^2$ alone and $\tau_e$ fixed at zero or fitting of both $S^2$ and $\tau_e$. The next two added an $R_{ex}$ term to the model-free formalism and provided fits to either all three parameters ($S^2$, $\tau_e$, and $R_{ex}$) or just $S^2$ and $R_{ex}$. The extended form of the model-free formalism served as the final representation of the spectral density function, fitting to the parameters $S^2$, $S_s^2$, and $\tau_e$.

The various representations of the spectral density function described above, all based on the Lipari and Szabo formalism, have been widely used and provide a generally acceptable framework for interpreting $^{15}$N relaxation data for proteins. However, there are several known limitations, including the inherent assumptions about the functional form of the spectral density function, the insensitivity of $S^2$ to motions slower than the nanosecond time scale, and the difficulty evaluating the exact physical meaning of $\tau_e$. To circumvent these limitations, several elegant procedures employing full and reduced spectral density mapping have been proposed (Peng & Wagner, 1992; Farrow *et al*., 1995; Ishima & Nagayama, 1995; Lefèvre *et al*., 1996). In the current study, we were more concerned with identifying patterns of relative mobility throughout the sequence and changes on ligand binding; we were less concerned with determining the exact physical meaning of specific values of a given motional parameter. Therefore, with the above limitations in mind, we considered the various Lipari and Szabo analyses described above to be adequate for the current study.

## RESULTS

*$^1$H/$^{15}$N HSQC Spectra and Resonance Assignments*. Backbone amide $^1$H and $^{15}$N assignments at 25 °C were established for 119 of the 131 residues of both apo and holo I-FABP. In previous studies, the $^1$H, $^{13}$C, and $^{15}$N chemical shift assignments for I-FABP complexed with palmitate at 37 °C (Hodsdon *et al.*, 1995, 1996) and apo I-FABP at 33 °C (Hodsdon & Cistola, 1997) were reported. In order to assign backbone amide resonances at 25 °C for the current study, a series of 2D $^1$H−$^{15}$N HSQC experiments were collected at temperature values of 37, 33, 29, and 25 °C. With a few exceptions, backbone amide resonance assignments easily migrated across the temperature range. A 3D $^{15}$N TOCSY-HMQC spectrum was aquired at 25 °C to confirm and/or establish any remaining assignments. In the

original assignment of apo I-FABP at 33 °C, backbone $^1H/^{15}N$ resonances were missing for 23 residues (Hodsdon & Cistola, 1997), 11 more than were missing in a nearly identical study of holo protein (Hodsdon *et al.*, 1995). In the current study, we were able to observe these 11 missing resonances by using gradient-enhanced pulse sequences designed to minimize saturation of the solvent resonance and by decreasing the temperature from 33 to 25 °C to lower the amide hydrogen exchange rate. Figure 2 displays the 25 °C $^1H/^{15}N$ HSQC spectra of apo (panel A) and holo (panel B) I-FABP. The backbone amide assignments used in the present study are labeled in the figure and are available as Supporting Information.

*Amide Hydrogen Exchange Measured by Saturation Transfer*. The effect of bound ligand on the rate of amide hydrogen exchange at 25 °C was assessed by observing the transfer of saturation from the solvent resonance to backbone amides. The relative intensity of $^1H/^{15}N$ correlations collected with and without solvent presaturation can be used to monitor hydrogen exchange rates which are on the order of the longitudinal relaxation rate ($T_1^{-1}$) of the amide proton (Gryk *et al.*, 1995). A comparison of saturation transfer ratios has been used to monitor changes in the local stability of protein structural units (Gryk & Jardetzky, 1996). The use of hydrogen exchange rates to gauge protein stability relies on a model developed by Englander and Kallenbach (1984), where local unfolding events disrupt backbone hydrogen-bonding interactions; exchange with solvent hydrogens is thought to occur from this manifold of locally and globally unfolded states.

Gradient-enhanced 2D $^1H-^{15}N$ HSQC spectra were accumulated for I-FABP with and without solvent presaturation during the relaxation delay. The relative peak intensities are plotted in Figure 3A for apo (filled circles) and holo I-FABP (open circles). For both forms of the protein, a decrease in peak intensity due to saturation transfer was observed for residues 27−36. However, for apo I-FABP, the decrease was accentuated and two additional locations of rapid hydrogen exchange were observed: residues N54−R56 and S71−T76. The difference in saturation transfer between apo and holo I-FABP is displayed in Figure 3B such that a positive difference value implies decreased protection from hydrogen exchange in the absence of fatty acid. The residues exhibiting a difference greater than one standard deviation from the average were V26−N35, N54 and F55, and S71−G75. These three portions of the sequence with decreased protection correspond to a single region of the tertiary structure corresponding to most of α-helix II, the α-II/β-B linker, and the C−D and E−F turns (Figure 1).

*Amide $^{15}N$ NMR Relaxation Parameters*. Peak intensities from the duplicate series of $T_1$ and $T_2$ relaxation spectra were normalized according to the intensity of their first data point. Combined, they were adequately fit by a two-parameter single-exponential decay (eq 1) resulting in low $\chi^2$ values and narrow 95% support-plane confidence limits. A three-parameter function did not result in a significantly better fit to the data. Typically, the additional parameter, describing a constant baseline offset, was insignicant in that its confidence limits contained a decay to an ordinate of zero.

The distribution of $^{15}N$ $T_1$ values along the protein sequence is plotted in Figure 4. The values averaged 438.1 and 439.7 ms for apo and holo protein, respectively, with average 95% confidence limits of 40.7 and 36.5 ms,

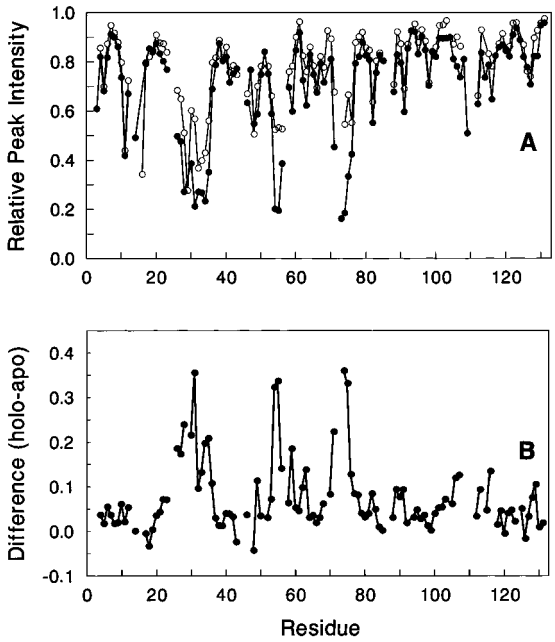


FIGURE 3: (A) Relative $^1H-^{15}N$ peak intensities with and without presaturation of the solvent resonance along the sequence of apo (filled circles) and holo (open circles) I-FABP. (B) Difference (holo − apo) between relative peak intensities for the two ligation states plotted such that a positive value denotes an increase in saturation transfer in the absence of ligand. In panel B, the average difference for all residues (±standard deviation) was 0.074 ± 0.082. Those residues with differences greater than one standard deviation above the mean are listed in the text.

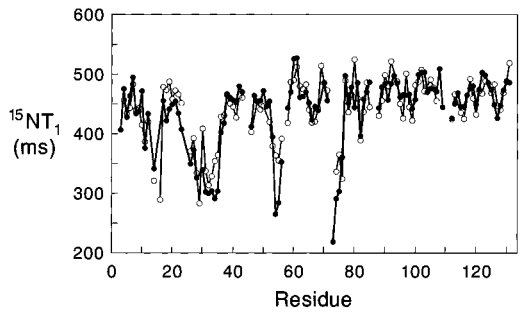


FIGURE 4: Distribution of the measured $^{15}N$ $T_1$ relaxation time values along the sequence of apo (filled circles) and holo (open circles) I-FABP. The average values for apo and holo I-FABP were 438.1 and 439.7 ms, with average 95% confidence limits of 40.7 and 36.5 ms, respectively.

respectively. The residues in apo I-FABP that exhibited $T_1$ values lower than these limits were N11, Y14, V26−N35, S53−R56, A73−T76, and W82. In holo I-FABP, a similar pattern was observed, but the magnitudes of the decreases were generally attenuated relative to the apo protein. The distributions of the $T_2$ and NOE relaxation parameters displayed a more uniform pattern of values along the protein sequence. Decreases were observed along the protein sequence in the same locations as the lower $T_1$ values. The decreases were small for apo I-FABP and mostly absent in the presence of ligand. The averages for the $T_2$ and NOE relaxation parameters were 116.4 ± 10.3 (apo $T_2$), 124.9 ± 7.9 (holo $T_2$), 0.74 ± 0.04 (apo NOE), and 0.76 ± 0.03 (holo NOE). The complete set of backbone amide $^{15}N$ $T_1$, $T_2$, and $\{^1H\}^{15}N$ NOE parameters for apo and holo I-FABP is available as Supporting Information.

*Spectral Density Function Analysis*. Analysis of the $^{15}N$ NMR relaxation parameters began with the determination

of the optimal overall correlation time ($\tau_m$) for the molecules. Using software developed by Farrow *et al.* (1994), all residues were simultaneously fit to a simple model-free formalism (eq 7) by iterating a grid search through a range of $\tau_m$ values. Because the global optimization considers the simplest model for the spectral density function, only residues generating an adequate fit were used at this stage. In the first iteration of the procedure, residues were selected on the basis of the ratio of $T_1/T_2$. Provided that $\tau_e < 100$ ps, $\tau_m > 1$ ns, and $T_2$ is not shortened by chemical exchange, $T_1/T_2$ is effectively dependent only on $\tau_m$ (Kay *et al*., 1989). A majority of residues in apo and holo I-FABP shared similar $T_1/T_2$ ratios; those more than one standard deviation outside the mean were excluded in this initial analysis. For residues with $T_1/T_2$ ratios far greater than the mean, conformational exchange was probably contributing to a reduction in $T_2$. Residues with $T_1/T_2$ ratios far lower than the mean were probably more correctly modeled by the two-time scale spectral density function.

Using the inital $\tau_m$ value, all residues were individually fit to each of the five representations of the spectral density described in Materials and Methods. A second grid search was then performed to determine the globally optimum $\tau_m$ using only those residues which were satisfactorily fit by the two-parameter model-free formalism. A total of 84 residues were globally optimized to a $\tau_m$ of 6.7 ns for apo I-FABP, and 67 residues were used to similarly determine a $\tau_m$ of 6.2 ns for holo I-FABP. Using these final $\tau_m$ values, all residues were again individually fit to each of the five spectral density functions.

The most appropriate spectral density function for each residue was selected using a procedure similar to that of Farrow *et al.* (1994). Initially, the four models based on the simple model-free formalism were considered, and the two-time scale spectral density function (eq 12) was disregarded. These spectral density functions were required to fit all three relaxation parameters within their 95% confidence limits. The effective correlation time for internal motions, $\tau_e$, and the conformational exchange term, $R_{ex}$, were included only if they individually satisfied two criteria: (1) the parameter values exceeded their calculated 95% confidence limits and (2) the equivalent model without their inclusion did not provide a satisfactory fit to the experimental data. In other words, these terms must have been both required for an adequate fit and significantly non-zero in order to have been considered. Lastly, the two-time scale spectral density function was considered only if none of the simpler models satisfied the above criteria. If none of the spectral density functions was adequate, then the model with the lowest $\chi^2$ value was tentatively assigned.

Tables 1 and 2 list the final spectral density function parameters for the residues in apo and holo I-FABP, respectively. For both forms of the protein, a majority of residues were fit by the simplest model-free formalism using either $S^2$ alone or $S^2$ with $\tau_e$. A total of 21 residues in apo I-FABP required a conformational exchange term, $R_{ex}$, and 9 residues were best fit by the two-time scale spectral density function ($S_s^2$, $S_f^2$, and $\tau_e$). Those residues fit by the two-time scale model were generally scattered throughout the protein sequence. However, residues containing an exchange term were clearly clustered to three distinct regions: residues V26−N35, S53−R56, and S71−G75. In holo I-FABP, 28 residues were best fit by the conformational exchange model and 11 by the two-time scale motion model. Unlike apo I-FABP, neither of these groups of residues displayed any clear pattern in their location throughout the sequence.

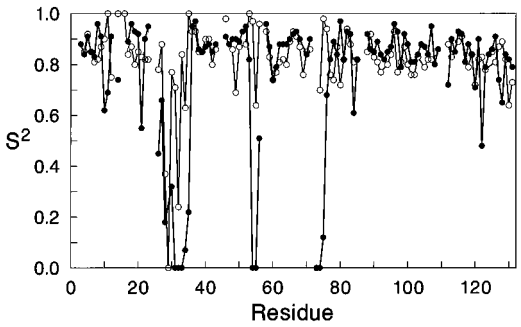


FIGURE 5: Distribution of the generalized order parameter, $S^2$, derived from a fit to the most appropriate spectral density function for each residue (Tables 1 and 2) along the sequence of apo (filled circles) and holo (open circles) I-FABP.

The generalized order parameter, $S^2$, served as a useful comparative tool for visualizing the motional characteristics of both ligation states of the protein. Figure 5 illustrates $S^2$ values along the sequence of I-FABP, and Table 3 lists the average order parameter values for various secondary structure elements. A majority of the residues are characterized by order parameters greater than 0.8 with an overall average (± the 95% confidence limit) of 0.76 ± 0.07 and 0.82 ± 0.04 for apo and holo I-FABP, respectively. Three distinct segments in apo I-FABP, seen in both Figure 5 and Table 3, display low order parameters. Again, these residues are in a single region comprised of helix α-II, the α-II/$\beta$-B linker, and the C−D and E−F turns. Although the parameters derived from the model-free description of the spectral density function cannot be interpreted according to a unique type of motion, low order parameter values are consistent with less restricted motions on the nanosecond to picosecond time scale (Lipari & Szabo, 1982a,b). In the liganded form of the protein, fewer residues (R28, K29, and A32) display very low order parameters. A direct comparison of secondary structure elements in Table 3 reveals that, on average, helix α-II, linker α-II/$\beta$-B, and turns $\beta$-C/$\beta$-D and $\beta$-E/$\beta$-F are characterized by a significant increase in order parameter values upon fatty acid binding.

It should be noted that sizable errors were observed for residues displaying order parameters near zero (Tables 1 and 2). The errors were not so large that the distributions of probable values between these residues and the rest of the protein overlapped. Rather, the increase in the calculated 95% confidence limits implied a decreased quality of fit. Combined with the difficulty in uniquely interpreting the model-free parameters, this decreased precision prevents a clear understanding of the specific nature of the protein motions giving rise to low $S^2$ values. However, it seems likely that in apo I-FABP residues displaying low order parameters undergo motions that are more random and less correlated with the rest of the protein and that ligand binding induces an ordering in these residues resulting in significantly higher $S^2$ values.

The residues requiring conformational exchange terms generally coincided with those with low order parameters. Quantitating the difference in exchange terms between apo and holo I-FABP was complicated by differences in the selection of the most appropriate spectral density function for a given residue (Tables 1 and 2). Therefore, as an

Table 1: Spectral Density Function Parameters for Apo I-FABP[a]

| | $S^2$ | $\tau_e$ | $R_{ex}$ | $\tau_s$ | $S_f^2$ | | $S^2$ | $\tau_e$ | $R_{ex}$ | $\tau_s$ | $S_f^2$ |
|---|---|---|---|---|---|---|---|---|---|---|---|
| A1 | | | | | | D67 | 0.93 (0.04) | | | | |
| F2 | | | | | | F68 | 0.90 (0.03) | 0.05 (0.03) | | | |
| D3 | 0.88 (0.08) | 1.72 (1.28) | | | | A69 | | | | | |
| G4 | 0.84 (0.02) | 0.04 (0.03) | | | | Y70 | 0.84 (0.02) | | | | |
| T5 | 0.91 (0.02 | | | | | S71 | 0.90 (0.06) | | 1.67 (0.56) | | |
| W6 | 0.85 (0.02) | | | | | L72 | | | | | |
| K7 | 0.83 (0.01) | | | | | A73 | 0.00 (0.05) | 5.13 (0.70) | 6.56 (2.30) | | |
| V8 | 0.96 (0.02) | | | | | D74 | 0.00 (0.45) | 6.70 (3.20) | 8.10 (1.85) | | |
| D9 | 0.91 (0.02) | | | | | G75 | 0.12 (0.33) | 6.70 (2.17) | 4.88 (1.31) | | |
| R10 | 0.62 (0.07) | | | 4.18 (1.50) | 0.81 (0.02) | T76 | 0.68 (0.15) | 5.96 (2.81) | | | |
| N11 | 0.69 (0.20) | 6.70 (2.85) | | | | E77 | 0.82 (0.02) | 0.06 (0.02) | | | |
| E12 | 0.91 (0.02) | | | | | L78 | 0.89 (0.02) | | | | |
| N13 | | | | | | T79 | 0.84 (0.02) | 0.03 (0.02) | | | |
| Y14 | 0.74 (0.15) | | | 6.70 (3.33) | 1.00 (0.09) | G80 | 0.97 (0.03) | | | | |
| E15 | | | | | | T81 | 0.82 (0.03) | 0.03 (0.01) | | | |
| K16 | | | | | | W82 | 0.93 (0.02) | | | | |
| F17 | 0.89 (0.02) | | | | | T83 | 0.92 (0.02) | | | | |
| M18 | 0.96 (0.03) | | | | | M84 | 0.61 (0.06) | | | 4.24 (2.04) | 0.81 (0.03) |
| E19 | 0.93 (0.02) | | | | | E85 | 0.82 (0.02) | 0.04 (0.01) | | | |
| K20 | 0.92 (0.04) | | | | | G86 | | | | | |
| M21 | 0.55 (0.10) | | | 6.07 (1.63) | 0.81 (0.04) | N87 | | | | | |
| G22 | 0.90 (0.03) | | | | | K88 | 0.92 (0.02) | 0.09 (0.07) | | | |
| I23 | 0.95 (0.03) | | | | | L89 | 0.86 (0.02) | 0.06 (0.04) | | | |
| N24 | | | | | | V90 | 0.85 (0.01) | | | | |
| V25 | | | | | | G91 | 0.89 (0.02) | | | | |
| V26 | 0.45 (0.38) | 3.86 (2.12) | 2.02 (1.71) | | | K92 | 0.84 (0.02) | | | | |
| K27 | 0.66 (0.22) | 3.47 (1.73) | 2.10 (1.02) | | | F93 | 0.82 (0.02) | 0.02 (0.01) | | | |
| R28 | 0.18 (0.31) | 3.98 (1.70) | 3.34 (1.46) | | | K94 | 0.85 (0.01) | | | | |
| K29 | | | | | | R95 | 0.87 (0.04) | | | | |
| L30 | 0.32 (0.25) | 3.67 (1.04) | 5.45 (1.07) | | | V96 | 0.96 (0.03) | | | | |
| G31 | 0.00 (0.25) | 5.34 (1.43) | 4.94 (1.27) | | | D97 | 0.93 (0.02) | | | | |
| A32 | 0.00 (0.21) | 6.39 (1.04) | 6.15 (1.01) | | | N98 | 0.79 (0.02) | 0.02 (0.01) | | | |
| H33 | 0.00 (0.20) | 3.86 (0.63) | 5.19 (1.03) | | | G99 | 0.92 (0.02) | | | | |
| D34 | 0.07 (0.29) | 6.70 (1.61) | 3.84 (1.32) | | | K100 | 0.88 (0.02) | 0.03 (0.02) | | | |
| N35 | 0.22 (0.41) | 6.70 (3.12) | 2.58 (1.48) | | | E101 | 0.81 (0.01) | 0.02 (0.01) | | | |
| L36 | 0.95 (0.04) | | | | | L102 | 0.81 (0.01) | | | | |
| K37 | 0.97 (0.03) | | | | | I103 | 0.84 (0.02) | | | | |
| L38 | 0.86 (0.02) | 0.04 (0.04) | | | | A104 | 0.88 (0.02) | | | | |
| T39 | 0.85 (0.02) | 0.04 (0.02) | | | | V105 | 0.87 (0.02) | | | | |
| I40 | 0.87 (0. 02) | | | | | R106 | 0.84 (0.02) | | | | |
| T41 | 0.88 (0.02) | 0.03 (0.03) | | | | E107 | 0.95 (0.03) | | | | |
| Q42 | 0.85 (0.03) | 0.03 (0.03) | | | | I108 | 0.80 (0.01) | 0.02 (0.01) | | | |
| E43 | 0.88 (0.02) | 0.03 (0.03) | | | | S109 | 0.86 (0.02) | 0.03 (0.02) | | | |
| G44 | | | | | | G110 | | | | | |
| N45 | | | | | | N111 | | | | | |
| K46 | 0.91 (0.03) | | | | | E112 | 0.72 (0.09) | | | 2.67 (1.19) | 0.92 (0.05) |
| F47 | 0.88 (0.02) | | | | | L113 | 0.90 (0.03) | | | | |
| T48 | 0.90 (0.04) | | 2.19 (0.52) | | | I114 | 0.85 (0.01) | 0.03 (0.02) | | | |
| V49 | 0.90 (0.03) | | | | | Q115 | 0.93 (0.02) | | | | |
| K50 | 0.89 (0.02) | | | | | T116 | 0.92 (0.06) | | 2.43 (0.76) | | |
| E51 | 0.93 (0.03) | | | | | Y117 | 0.81 (0.02) | 0.05 (0.03) | | | |
| S52 | 0.95 (0.02) | | | | | T118 | 0.88 (0.02) | | | | |
| S53 | 0.82 (0.15) | 2.46 (1.84) | 1.22 (0.79) | | | Y119 | 0.84 (0.02) | | | | |
| N54 | 0.00 (0.46) | 6.70 (2.91) | 4.98 (1.84) | | | E120 | 0.71 (0.09) | | | 6.70 (2.50) | 0.86 (0.03) |
| F55 | 0.00 (0.20) | 5.54 (1.34) | 4.62 (0.92) | | | G121 | 0.90 (0.02) | 0.06 (0.04) | | | |
| R56 | 0.51 (0.28) | 4.43 (2.02) | 4.10 (1.60) | | | V122 | 0.48 (0.05) | | | 5.62 (1.44) | 0.73 (0.02) |
| N57 | | | | | | E123 | 0.79 (0.01) | 0.03 (0.01) | | | |
| I58 | 0.96 (0.02 | 0.27 (0.12) | | | | A124 | 0.84 (0.02) | | | | |
| D59 | 0.87 (0.04) | | 1.60 (0.45) | | | K125 | 0.86 (0.03) | | 2.45 (0.58) | | |
| V60 | 0.74 (0.03) | 0.02 (0.02) | | | | R126 | 0.91 (0.01) | 0.05 (0.03) | | | |
| V61 | 0.79 (0.02) | 0.02 (0.01) | | | | I127 | 0.74 (0.08) | | | 6.70 (3.00) | 0.90 (0.07) |
| F62 | 0.88 (0.02) | 0.04 (0.04) | | | | F128 | 0.65 (0.06) | | | 6.70 (1.94) | 0.85 (0.04) |
| E63 | 0.88 (0.02) | | | | | K129 | 0.84 (0.02) | 0.06 (0.02) | | | |
| L64 | 0.88 (0.03) | | | | | K130 | 0.82 (0.03) | 0.03 (0.01) | | | |
| G65 | 0.90 (0.02) | | | | | E131 | 0.79 (0.02) | 0.06 (0.01) | | | |
| V66 | 0.92 (0.03) | | | | | | | | | | |

[a] Values in parentheses represent the 95% confidence limits as described in the text.

alternative approach, we fit every residue in both proteins to a single model of the spectral density function ($S^2$, $\tau_e$, and $R_{ex}$; eq 10). Most residues fit well to this model, and as expected, many of the conformational exchange terms were essentially zero. The distributions of $S^2$ and $R_{ex}$ values derived from this analysis are plotted in Figure 6. The patterns of $S^2$ values are similar to those presented in Figure 5, indicating a general agreement between this single-model interpretation of the data and the more detailed analysis described previously. Therefore, the model containing a

Table 2: Spectral Density Function Parameters for Holo I-FABP[a]

| | $S^2$ | $\tau_e$ | $R_{ex}$ | $\tau_s$ | $S_f^2$ | | $S^2$ | $\tau_e$ | $R_{ex}$ | $\tau_s$ | $S_f^2$ |
|---|---|---|---|---|---|---|---|---|---|---|---|
| A1 | | | | | | D67 | 0.91 (0.03) | | | | |
| F2 | | | | | | F68 | 0.87 (0.03) | | | | |
| D3 | | | | | | A69 | 0.76 (0.02) | | 1.92 (0.37) | | |
| G4 | 0.85 (0.02) | 0.04 (0.02) | | | | Y70 | 0.85 (0.03) | 0.02 (0.02) | | | |
| T5 | 0.92 (0.02) | | | | | S71 | 0.86 (0.01) | 0.03 (0.02) | | | |
| W6 | 0.85 (0.02) | | | | | L72 | | | | | |
| K7 | 0.81 (0.02) | | 0.97 (0.31) | | | A73 | | | | | |
| V8 | 0.82 (0.03) | 0.02 (0.02) | | | | D74 | 0.70 (0.10) | | | 6.20 (1.97) | 1.00 (0.06) |
| D9 | 0.87 (0.02) | | | | | G75 | 0.98 (0.02) | | | | |
| R10 | 0.90 (0.02) | | | | | T76[b] | 0.94 (0.05) | | | 6.20 (2.73) | 1.00 (0.08) |
| N11 | 1.00 (0.04) | | 1.06 (0.39) | | | E77 | 0.76 (0.03) | 0.02 (0.01) | | | |
| E12 | 0.75 (0.05) | | | 6.20 (2.17) | 0.89 (0.06) | L78 | 0.74 (0.07) | | | 6.20 (2.71) | 0.86 (0.06) |
| N13 | | | | | | T79 | 0.87 (0.02) | | | | |
| Y14[b] | 1.00 (0.00) | | 0.46 (0.25) | | | G80 | 0.72 (0.02) | 0.02 (0.01) | | | |
| E15 | | | | | | T81 | 0.82 (0.03) | | | | |
| K16 | 1.00 (0.00) | | 0.76 (1.52) | | | W82 | 0.94 (0.03) | | | | |
| F17 | 0.84 (0.02) | | | | | T83 | 0.88 (0.01) | | | | |
| M18 | 0.87 (0.02) | | | | | M84 | 0.81 (0.01) | | | | |
| E19 | 0.80 (0.04) | | 1.06 (0.44) | | | E85 | 0.82 (0.02) | 0.04 (0.03) | | | |
| K20 | 0.85 (0.01) | | 1.47 (0.39) | | | G86 | | | | | |
| M21 | 0.83 (0.02) | | 1.12 (0.41) | | | N87 | | | | | |
| G22 | 0.82 (0.02) | | | | | K88 | 0.85 (0.03) | 0.06 (0.03) | | | |
| I23 | 0.82 (0.02) | 0.02 (0.02) | | | | L89 | 0.92 (0.03) | | | | |
| N24 | | | | | | V90 | 0.83 (0.02) | | | | |
| V25 | | | | | | G91 | 0.81 (0.01) | | 0.80 (0.23) | | |
| V26 | 0.78 (0.08) | | | 2.31 (1.13) | 1.00 (0.02) | K92 | 0.77 (0.01) | | | | |
| K27 | 0.88 (0.04) | | | 1.35 (1.18) | 1.00 (0.02) | F93 | | | | | |
| R28 | 0.37 (0.21) | 5.53 (1.26) | 3.00 (0.74) | | | K94 | 0.80 (0.01) | | 0.84 (0.31) | | |
| K29 | 0.00 (0.44) | 6.20 (2.41) | 4.93 (1.64) | | | R95 | 0.84 (0.02) | | | | |
| L30 | 0.77 (0.11) | | | 1.48 (1.00) | 0.97 (0.04) | V96 | 0.93 (0.02) | | | | |
| G31 | 0.71 (0.12) | 6.20 (2.70) | | | | D97 | 0.77 (0.03) | 0.01 (0.01) | 2.31 (0.34) | | |
| A32 | 0.24 (0.38) | 6.20 (2.53) | 2.74 (1.48) | | | N98 | 0.81 (0.01) | | | | |
| H33 | 0.84 (0.08) | | | 2.57 (1.72) | 1.00 (0.01) | G99 | 0.87 (0.02) | | | | |
| D34 | 0.63 (0.16) | 4.38 (2.39) | | | | K100 | 0.80 (0.02) | 0.01 (0.01) | 1.01 (0.14) | | |
| N35 | 1.00 (0.01) | | | | | E101 | 0.76 (0.01) | | | | |
| L36 | 0.93 (0.03) | | | | | L102 | 0.76 (0.02) | 0.02 (0.01) | 0.87 (0.38) | | |
| K37 | 0.93 (0.02) | | | | | I103 | 0.83 (0.02) | | 0.73 (0.39) | | |
| L38 | 0.85 (0.01) | | | | | A104 | | | | | |
| T39 | 0.85 (0.01) | | | | | V105 | 0.79 (0.03) | 0.01 (0.01) | 1.43 (0.31) | | |
| I40 | 0.90 (0.01) | | | | | R106 | 0.82 (0.01) | | | | |
| T41 | 0.90 (0.02) | | | | | E107 | 0.82 (0.02) | | | | |
| Q42 | 0.80 (0.02) | | | | | I108 | | | | | |
| E43 | 0.86 (0.02) | 0.05 (0.02) | | | | S109 | | | | | |
| G44 | | | | | | G110 | | | | | |
| N45 | | | | | | N111 | | | | | |
| K46 | 0.98 (0.02) | | | | | E112 | 0.88 (0.01) | 0.06 (0.03) | | | |
| F47 | | | | | | L113 | 0.83 (0.02) | | | | |
| T48 | 0.86 (0.04) | | 1.17 (0.38) | | | I114 | | | | | |
| V49 | 0.69 (0.09) | | | 6.20 (2.97) | 0.84 (0.07) | Q115 | 0.89 (0.02) | | | | |
| K50 | 0.87 (0.02) | | | | | T116 | 0.91 (0.02) | | | | |
| E51 | | | | | | Y117 | | | | | |
| S52 | 0.88 (0.02) | | | | | T118 | 0.79 (0.03) | 0.01 (0.01) | 1.79 (0.28) | | |
| S53 | 1.00 (0.00) | | | | | Y119 | 0.84 (0.03) | | | | |
| N54 | 0.97 (0.03) | | | | | E120 | 0.72 (0.06) | | | 6.20 (2.41) | 0.86 (0.05) |
| F55 | 0.64 (0.02) | 5.46 (2.06) | 1.92 (0.79) | | | G121 | 0.82 (0.03) | 0.02 (0.01) | 1.18 (0.32) | | |
| R56 | 0.96 (0.04) | | | | | V122 | 0.83 (0.02) | 0.01 (0.01) | 0.75 (0.32) | | |
| N57 | | | | | | E123 | 0.78 (0.01) | 0.02 (0.01) | | | |
| I58 | 0.93 (0.02) | | | | | A124 | | | | | |
| D59 | 0.83 (0.02) | | | | | K125 | 0.85 (0.01) | | | | |
| V60 | 0.74 (0.02) | 0.03 (0.01) | | | | R126 | 0.81 (0.04) | | 1.26 (0.39) | | |
| V61 | 0.77 (0.01) | | | | | I127 | 0.87 (0.03) | | 1.30 (0.35) | | |
| F62 | 0.81 (0.02) | 0.01 (0.01) | 0.97 (0.29) | | | F128 | 0.89 (0.02) | | | | |
| E63 | 0.82 (0.03) | | 0.94 (0.32) | | | K129 | 0.82 (0.02) | | | | |
| L64 | 0.80 (0.03) | | | | | K130 | 0.64 (0.04) | | | 2.57 (1.21) | 0.78 (0.02) |
| G65 | 0.89 (0.03) | | | | | E131 | 0.73 (0.01) | 0.05 (0.01) | 0.86 (0.27) | | |
| V66 | 0.93 (0.02) | | | | | | | | | | |

[a] Values in parentheses represent the 95% confidence limits as described in the text. [b] A few residues did not fit well to any of the five forms of the spectral density function. Therefore, the fit with the lowest $\chi^2$ value was chosen.

conformational exchange term provided a meaningful overall comparison of the dynamical properties of the apo and holo proteins.

Three distinct locations in the apo I-FABP sequence displayed evidence for some type of conformational exchange process that contributes to the transverse $^{15}N$ NMR relaxation

Table 3: Average Order Parameter Values for Secondary Structural Elements[a]

| | residues | apo I-FABP | holo I-FABP |
|---|---|---|---|
| helix | | | |
| α-I | 15−21 | 0.85 (0.04) | 0.86 (0.02) |
| α-II | 25−32 | 0.27 (0.27) | 0.54 (0.20) |
| strand | | | |
| *β*-A | 5−12 | 0.83 (0.05) | 0.86 (0.03) |
| *β*-B | 37−43 | 0.88 (0.02) | 0.87 (0.02) |
| *β*-C | 46−53 | 0.90 (0.04) | 0.88 (0.03) |
| *β*-D | 56−63 | 0.80 (0.06) | 0.84 (0.02) |
| *β*-E | 68−72 | 0.88 (0.03) | 0.83 (0.02) |
| *β*-F | 77−85 | 0.85 (0.03) | 0.82 (0.03) |
| *β*-G | 88−94 | 0.86 (0.02) | 0.83 (0.02) |
| *β*-H | 101−109 | 0.85 (0.02) | 0.80 (0.02) |
| *β*-I | 112−119 | 0.86 (0.03) | 0.86 (0.02) |
| *β*-J | 122−129 | 0.76 (0.04) | 0.84 (0.02) |
| reverse turns | | | |
| α-I/α-II | 22−24 | 0.92 (0.03) | 0.82 (0.02) |
| *β*-B/*β*-C | 44 and 45[b] | | |
| *β*-C/*β*-D | 54 and 55 | 0.00 (0.33) | 0.82 (0.12) |
| *β*-D/*β*-E | 64−67 | 0.91 (0.03) | 0.88 (0.03) |
| *β*-E/*β*-F | 73−76 | 0.20 (0.25) | 0.88 (0.06) |
| *β*-F/*β*-G | 86 and 87[b] | | |
| *β*-G/*β*-H | 95−100 | 0.89 (0.02) | 0.84 (0.02) |
| *β*-H/*β*-I | 110 and 111[b] | | |
| *β*-I/*β*-J | 120 and 121 | 0.81 (0.05) | 0.77 (0.04) |
| linkers | | | |
| *β*-A/α-I | 13 and 14 | 0.74 (0.15) | 1.00 (0.00) |
| α-II/*β*-B | 33−36 | 0.31 (0.24) | 0.85 (0.07) |

[a] Secondary structural elements are defined by the consensus chemical shift index of holo I-FABP (Hodsdon *et al*., 1995). Values in parentheses represent the 95% confidence limits as described in the text. [b] Because of rapid amide hydrogen exchange, order parameters are not available for some of the *β*-turn elements.

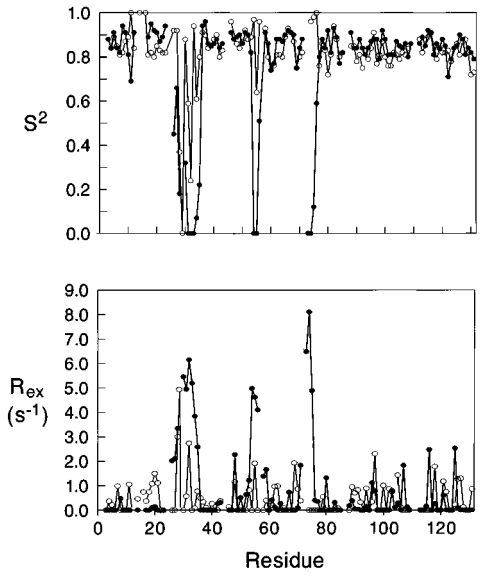


FIGURE 6: Distribution of the generalized order parameter, $S^2$, and the conformational exchange term, $R_{ex}$, derived from fitting every residue in apo (filled circles) and holo (open circles) I-FABP to a fixed model of the spectral density function containing the paramters $S^2$, $\tau_e$, and $R_{ex}$.

time (Figure 6). The specific interpretation of the $R_{ex}$ term is complicated and depends on knowledge of all the states involved in the exchange process and their chemical shift differences (Palmer *et al*., 1991). However, as described in Materials and Methods, the presence of a non-zero $R_{ex}$ parameter in the fit of the relaxation data to the spectral density function implies that an exchange process occurring on the microsecond to millisecond time scale.

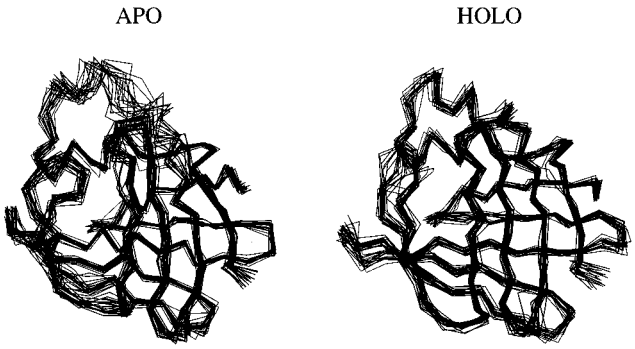


FIGURE 7: Ensembles of 20 superposed $C_\alpha$ backbone traces for apo I-FABP (Hodsdon & Cistola, 1997) and I-FABP complexed with palmitate (Hodsdon *et al.*, 1996). The apo ensemble (left) was characterized by increased average pairwise $C_\alpha$ deviations that were most apparent in residues 29−36 and 54−57.

## DISCUSSION

To date, rat I-FABP is the only member of the iLBP family for which the NMR solution structures and backbone dynamics have been characterized in the presence and absence of bound ligand. Therefore, the results for I-FABP provide a unique opportunity to assess the effect of bound ligand on the solution-state properties of the protein at the atomic level. In the present study, the backbone mobility of I-FABP in the presence and absence of bound fatty acid was directly compared using NMR measurements of amide $^1$H exchange rates and $^{15}$N NMR relaxation rates. In both types of measurements, we observed that a single region of the tertiary structure had unusual dynamic properties. Residues in α-helix II, the α-II/*β*-B linker, and the C−D and E−F turns were more mobile than other parts of the protein, particularly in the absence of bound fatty acid. Within helix II, the increased mobility was most pronounced in the C-terminal portion. The local disorder in apo I-FABP was shown by higher rates of amide $^1$H exchange, lower order parameters, and sizable conformational exchange terms. In contrast, the remainder of the protein backbone was characterized by slow amide hydrogen exchange, high order parameters, and vanishing conformational exchange terms for both ligation states of the protein.

We previously established evidence for a discrete region of backbone disorder in apo I-FABP by comparing its NMR solution structure with that of the protein complexed with palmitate (Figure 7). The apparent backbone disorder in the apo structure was shown by local increases in the average pairwise Cα deviations and differences in the consensus $^1$H/$^{13}$C chemical shift indices for the apo and holo proteins (Hodsdon & Cistola, 1997). In addition, some amide $^1$H resonances were selectively absent in triple-resonance spectra of the apo, but not holo, proteins collected under nearly identical conditions. The apparent disorder was most pronounced in residues K29−L36 and N54−N57 and coincided with the region of increased backbone mobility as determined in the current study. Thus, the dynamic measurements reinforced conclusions drawn from comparisons of the chemical shifts and NOE-derived structures and indicated that the local variability in the ensemble of apo NMR structures represents increased backbone mobility in a specific region of the protein.

The cumulative evidence for a localized region of backbone disorder in apo I-FABP is compelling and is sum-

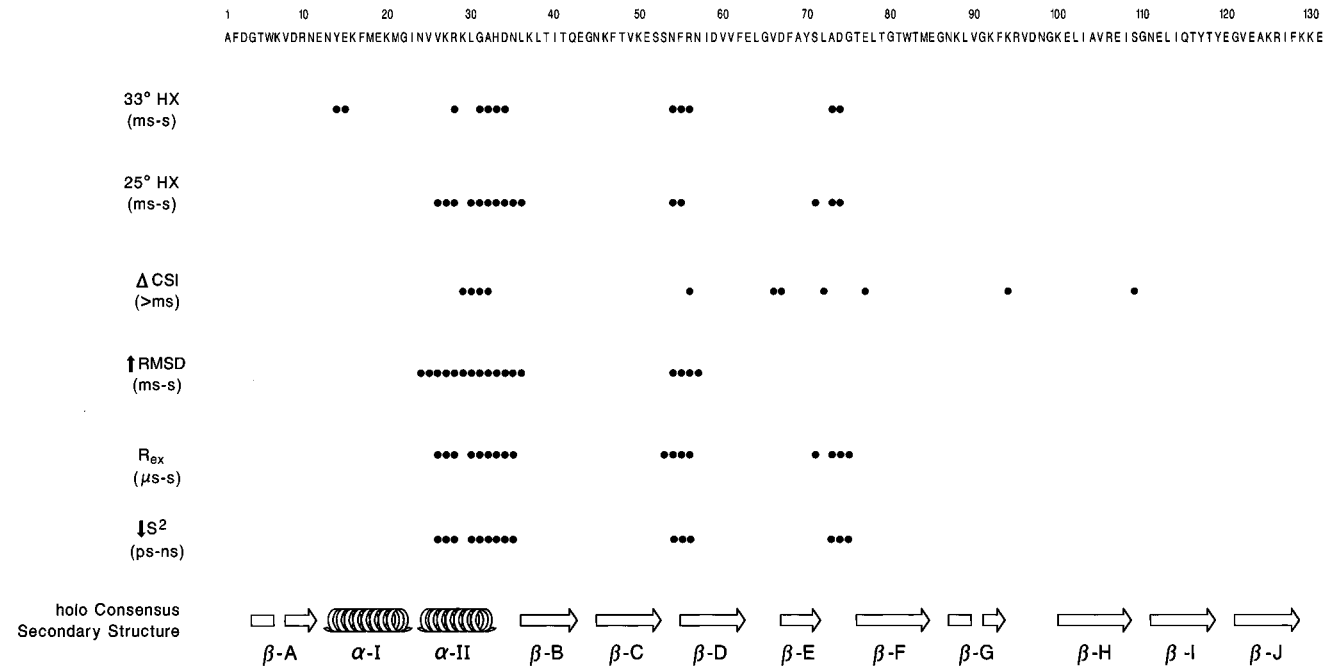


FIGURE 8: Summary of the NMR evidence for discrete disorder in the backbone of apo I-FABP. The dots in each row represent the following: 33° HX, positions of backbone amide protons missing in triple-resonance spectra of apo but not holo I-FABP (Hodsdon & Cistola, 1997); 25° HX, positions of backbone amide protons less protected in the apo state (Figure 3B); ΔCSI, residues exhibiting disorder in the consensus $^1H/^{13}C$ chemical shift indices of apo but not holo I-FABP (Hodsdon & Cistola, 1997); ↑RMSD, regions of increased pairwise Cα deviations in the ensemble of apo I-FABP NMR structures (Hodsdon & Cistola, 1997); $R_{ex}$, positions requiring exchange term for analysis of relaxation for apo I-FABP (Table 1); and $S^2$, residues with low $S^2$ values for apo I-FABP (Table 1).

marized in Figure 8. The regions with increased backbone mobility, as determined from relaxation measurements, correlate well with the regions of increased backbone deviations in the NMR structure ensemble. A somewhat similar correlation has been observed with interleukin-4 (Redfield *et al*., 1992).

Several other proteins have been observed to undergo changes in backbone mobility upon ligand binding. Examples include FK506 binding protein (Cheng *et al*., 1994), acyl-coenzyme A binding protein (Rischel *et al*., 1994), and HIV protease (Nicholson *et al*., 1995). In at least one case, single-stranded DNA binding to a topoisomerase domain (Yu *et al.*, 1996), several regions of the protein backbone became *less* ordered upon ligand binding.

*Dynamic Portal Hypothesis.* We recently presented a revised hypothesis suggesting that the localized region of backbone disorder in I-FABP constitutes a dynamic, flexible portal that permits the entry of ligand (Hodsdon & Cistola, 1997). According to this hypothesis, apo I-FABP exists as a manifold of locally disordered and ordered states in solution, and the disordered states are characterized by a decoupling of long-range interactions between helix II and the C−D turn and a fraying of the distal half of helix II. We proposed that the binding of fatty acid shifts the order−disorder equilibrium toward the ordered, closed state by stabilizing a series of cooperative interactions resembling a helix capping box (Aurora *et al.*, 1994; Hodsdon & Cistola, 1997).

The concept of a ligand entry portal was originally proposed by Sacchettini *et al.* (1989, 1992) and was based on a detailed comparison of the high-resolution X-ray crystal structures of I-FABP with and without bound fatty acids. In the X-ray structures, the backbone conformations of the apo and holo forms were well-ordered and essentially superimposable [see Figure 14 of Scapin *et al*. (1992)]. None of the crystal structures exhibited any obvious openings large enough for the entry and exit of fatty acid. However, a region bounded by the α-helices and the C−D and E−F turns exhibited the least dense packing of atoms and was viewed as a likely location for a ligand entry portal (Sacchettini *et al.*, 1989). Also, a narrow solvent channel connecting the interior cavity with the external solvent was observed in this region. The aromatic ring of F55 appeared to serve as a lid to this channel, and its side chain conformation varied in the presence and absence of fatty acids. On the basis of these studies, the binding of fatty acid was thought to be accompanied primarily by the displacement of ordered water molecules without prominent conformational changes in the protein (Sacchettini *et al.*, 1992; Banaszak *et al*., 1994).

A somewhat different hypothesis was that ligand binding involves a significant change in the conformation of the protein backbone. This view was based on the differing susceptibilities of several lipid-binding proteins to limited proteolysis in the presence and absence of ligand (Jamison *et al.*, 1994). Additional evidence for a conformational change came from studies comparing the properties of a helix-less variant of I-FABP with those of the wild-type protein (Kim *et al.*, 1996; Cistola *et al.*, 1996). A rate-limiting step was observed in the association of oleate with wild-type I-FABP but not with the helix-less variant. This rate-limiting process was interpreted as a conformational change involving the helical region that allowed the ligand access to the internal binding cavity (Cistola *et al.*, 1996).

The dynamical picture of I-FABP provided by the current NMR results lends support for some features of the earlier hypotheses while providing new insights into the ligand entry and exit mechanism. The region of discrete backbone disorder and increased mobility in the NMR structures,

although not observed in the X-ray structure,[2] coincides with the deduced location of the ligand entry portal (Sacchettini *et al*., 1989). The current view of the portal is that of a flexible, dynamic region of the protein backbone rather than a relatively fixed channel that is modulated by the rotation of a few side chains. Also, the NMR results are consistent with a conformational change associated with ligand binding. We envision the conformational change as an order−disorder transition with a fraying of the distal half of helix II and a decoupling of long-range interactions with the C−D turn (Hodsdon & Cistola, 1997), rather than hinged rotation of the entire helix−turn−helix domain relative to the rest of the protein.

The NMR solution structure of the apo form of porcine I-LBP has recently been determined using 2D $^1$H NMR methods (Lücke *et al*., 1996). Porcine I-LBP shares 21% sequence identity with rat I-FABP and has a different ligand specificity, preferring bile salts over fatty acids. Lücke *et al*. propose that I-LBP may have increased flexibility in the $\beta$-sheet region of the protein compared with other members of the lipid-binding protein family and that the increased flexibility may explain the difference in ligand specificity. This $\beta$-sheet flexibility was not observed in the ensemble of NMR structures but inferred from NOEs, amide $^1$H chemical shift values, and the rate of disappearence of amide $^1$H resonances in $D_2O$. This proposed flexibility in the $\beta$-sheet domain of I-LBP is different from the backbone disorder and increased mobility in the portal region of I-FABP, as described in the current study.

Like I-FABP, the ensemble of NMR structures for apo I-LBP also exhibited increased variability in α-helix II and the C−D turns (Lücke *et al*., 1996). Since the backbone dynamics of I-LBP have not yet been characterized, it is not yet known whether this variability represents increased disorder or simply a lack of conformational restraints in this region of the protein. Also, the NMR structure of the holo form of I-LBP has not been determined, and it is not yet known whether this variability is affected by the presence of ligand. Nevertheless, the variability could represent a phenomenon similar to that described here for I-FABP and may indicate that the apo forms of other members of the protein family also exhibit discrete backbone disorder in the portal region. The ensemble of NMR structures of bovine heart FABP also showed variability in helix II, but unlike the case for I-FABP, the variability in the structures was observed in the presence of bound ligand (Lassen *et al*., 1995; Hodsdon *et al*., 1996).

*Implications for Fatty Acid Transfer and Targeting*. The research of Storch and co-workers has elucidated distinct mechanisms by which different iLBPs transfer fatty acid to phospholipid membranes *in vitro* (Kim & Storch, 1992a,b; Wootan *et al*., 1993). Liver FABP releases ligand to the aqueous milieu prior to insertion into membranes. In contrast, the adipocyte, heart, and intestinal proteins transfer fatty acid during direct, effective collisions with acceptor membranes. Ionic interactions between charged residues in the helical domain and membrane phospholipids appear to govern these collisional interactions. Fatty acid transfer rates from A-LBP and H-FABP increase as a function of membrane negative charge and decrease with positive charge. A single lysine side chain, located at position 22 in helix α-I, appears to be responsible for the ionic interaction between H-FABP and phospholipid membranes (Herr *et al*., 1996). Any mutation or modification of this residue results in a slower overall rate of fatty acid transfer and a virtual absence of sensitivity to membrane charge. The addition of a second lysine at position 28 of helix α-II of H-FABP, naturally present in A-LBP, increased the fatty acid transfer rate 4-fold and results in agreement with the rates observed for A-LBP. This residue is one of the few sequence dissimilarities in the helical domains of A-LBP and H-FABP, whereas there is no sequence similarity with L-FABP in this region. These results demonstrate that ionic interactions involving residues in the helical domain regulate the collisional mechanism of ligand transfer observed in some iLBPs.

The effect of mutations on the transfer of fatty acid to phospholipid membranes was specific to the helical domain of H-FABP since modifications of $\beta$-sheet residues, with one notable exception, had no effect. Mutation of K59, located in the C−D turn of H-FABP, increased the rate of transfer by 2-fold with no affect on the sensitivity to membrane charge. A double mutation at positions K22 and K59 resulted in a roughly additive effect on the transfer rate, suggesting that at least two distinct structural regions may independently affect ligand transfer. The authors speculated on a possible multiphase mechanism for fatty acid transfer. First, protein−membrane collisions, governed by ionic interactions with specific residues in the helical domain, are required. This may be followed by a conformational transition or "repositioning" involving the C−D turn and resulting in a "hinged opening" of the portal region to release ligand.

Given the collisional transfer mechanism (Hsu & Storch, 1996), it is tempting to speculate about the possible role of backbone flexibility in the intracellular function of I-FABP. We suggest that the order−disorder transition observed in the NMR results for I-FABP may correspond to the "conformational transition" postulated by Storch and co-workers. Thus, the collision of the fatty acid−protein complex with acceptor membranes may shift the order−disorder equilibrium toward the disordered state(s) and facilitate the release of ligand to the acceptor. In this manner, I-FABP may be able to adjust its ligand dissociation rate depending on its interactions with various organelles. In the cytoplasm, the fatty acid-protein complex would be more stable and optimized for ligand sequestration and transcytoplasmic diffusion. The dynamic portal would be in an essentially closed state, with a lower fatty acid dissociation rate and higher affinity. However, during a collision with target sites, the cooperative interactions in the dynamic portal would be destabilized and the ligand dissociation rate would increase, facilitating ligand release. Hence, the ability of I-FABP to collide with target organelles and release fatty acid through a locally disordered region of the protein backbone may provide a mechanism for preferentially targeting fatty acids to certain organelles and metabolic pathways.

## ACKNOWLEDGMENT

The authors are indebted to Drs. Neil Farrow, Ranjith Muhandiram, and Lewis Kay of the University of Toronto for generously providing valuable advice and software for the relaxation analyses as well as source code for the pulse sequences. We also thank Drs. Chang-guo Tang for NMR advice and assistance and James Toner for the biosynthesis and assistance with the purification of the samples.

## SUPPORTING INFORMATION AVAILABLE

Five tables containing $^{1}H/^{15}N$ assignments for apo and holo I-FABP at 25 °C, complete $^{15}N$ NMR relaxation parameters for apo and holo I-FABP, and complete spectral density function analyses and parameters for apo and holo I-FABP (36 pages). Ordering information is given on any current masthead page.

## REFERENCES


Abragam, A. (1961) *Principles of Nuclear Magnetism*, Clarendon Press, Oxford.

Aurora, R., Srinivasan, R., & Rose, G. D. (1994) *Science 264*, 1126−1130.

Banaszak, L. J., Winter, N., Xu, Z., Bernlohr, D. A., Cowan, S., & Jones, T. A. (1994) *Adv. Protein Chem. 45*, 89−151.

Box, G. P., Hunter, W. G., & Hunter, J. S. (1978) *Statistics for Experimenters*, John Wiley & Sons, New York.

Cavanagh, J., Palmer, A. G., III, Wright, P. E., & Rance, M. (1991) *J. Magn. Reson. 91*, 429.

Cheng, J.-W., Lepre, C. A., & Moore, J. M. (1994) *Biochemistry 33*, 4093−4100.

Cistola, D. P., & Hall, K. B. (1995) *J. Biomol. NMR 5*, 415−419.

Cistola, D. P., Sacchettini, J. C., Banaszak, L. J., Walsh, M. T., & Gordon, J. I. (1989) *J. Biol. Chem. 264*, 2700−2710.

Cistola, D. P., Kim, K., Rogl, H., & Frieden, C. (1996) *Biochemistry 35*, 7559−7565.

Clore, G. M., Driscoll, P. C., Wingfield, P. T., & Gronenborn, A. M. (1990a) *Biochemistry 29*, 7387−7401.

Clore, G. M., Szabo, A., Bax, A., Kay, L. E., Driscoll, P. C., & Gronenborn, A. M. (1990b) *J. Am. Chem. Soc. 112*, 4989.

Englander, S. W., & Kallenbach, N. R. (1984) *Q. Rev. Biophys. 16*, 521−655.

Farrow, N. A., Muhandiram, R., Singer, A. U., Pascal, S. M., Kay, C. M., Gish, G., Shoelson, S. E., Pawson, T., Forman-Kay, J. D., & Kay, L. E. (1994) *Biochemsitry 33*, 5984−6003.

Farrow, N. A., Zhang, O., Szabo, A., Torchia, D. A., & Kay, L. E. (1995) *J. Biomol. NMR 6*, 153−162.

Gryk, M. R., & Jardetzky, O. (1996) *J. Mol. Biol. 255*, 204−214.

Gryk, M. R., Finucaine, M. D., Zheng, Z., & Jardetzky, O. (1995) *J. Mol. Biol. 246*, 618−627.

Herr, F. M., Aronson, J., & Storch, J. (1996) *Biochemistry 35*, 1296−1303.

Hiyama, Y., Niu, C., Silverton, J. V., Bavoso, A., & Torchia, D. A. (1988) *J. Am. Chem. Soc. 110*, 2378.

Hodsdon, M. E., & Cistola, D. P. (1997) *Biochemistry 36*, 1450−1460.

Hodsdon, M. E., Toner, J. J., & Cistola, D. P. (1995) *J. Biomol. NMR 6*, 198−210.

Hodsdon, M. E., Ponder, J. W., & Cistola, D. P. (1996) *J. Mol. Biol. 264*, 585−602.

Hsu, K. T., & Storch, J. (1996) *J. Biol. Chem. 271*, 13317−13323.

Ishima, R., & Nagayama, K. (1995) *Biochemistry 34*, 3162−3171.

Jakoby, M. G., Miller, K. R., Toner, J. J., Bauman, A., Cheng, L., Li, E., & Cistola, D. P. (1993) *Biochemistry 32*, 872−878.

Jamison, R. S., Newcomer, M. E., & Ong, D. E. (1994) *Biochemistry 33*, 2873−2879.

Kay, L. E., Torchia, D. A., & Bax, A. (1989) *Biochemistry 28*, 8972−8979.

Kay, L. E., Keifer, P., & Saarinen, T. (1992) *J. Am. Chem. Soc. 114*, 10663.

Kim, H. K., & Storch, J. (1992a) *J. Biol. Chem. 267*, 20051−20056.

Kim, H. K., & Storch, J. (1992b) *J. Biol. Chem. 267*, 77−82.

Kim, K., Cistola, D. P., & Frieden, C. (1996) *Biochemistry 35*, 7553−7558.

Lassen, D., Lücke, C., Kveder, M., Mesgarzadeh, A., Schmidt, J. M., Specht, B., Lezius, A., Spener, F., & Rüterjans, H. (1995) *Eur. J. Biochem. 230*, 266−280.

Lefevre, J.-F., Dayie, K. T., Peng, J. W., & Wagner, G. (1996) *Biochemistry 35*, 2674−2686.

Li, E., Locke, B., Yang, N. C., Ong, D. E., & Gordon, J. I. (1987) *J. Biol. Chem. 262*, 13773−13779.

Lipari, G., & Szabo, A. (1982a) *J. Am. Chem. Soc. 104*, 4546−4559.

Lipari, G., & Szabo, A. (1982b) *J. Am. Chem. Soc. 104*, 4559−4570.

Lowe, J. B., Sacchettini, J. C., Laposata, M., McQuillan, J. J., & Gordon, J. I. (1987) *J. Biol. Chem. 262*, 5931−5937.

Lücke, C., Zhang, F., Rüterjans, H., Hamilton, J. A., & Sacchettini, J. C. (1996) *Structure 4*, 785−800.

Markley, J. L., Horsley, W. J., & Klein, M. P. (1971) *J. Chem. Phys. 55*, 3604.

Muhandiram, D. R., & Kay, L. E. (1994) *J. Magn. Reson. Ser. B 103*, 203−216.

Nicholson, L. K., Yamazaki, T., Torchia, D. A., Grzesiek, S., Bax, A., Stahl, S. J., Kaufman, J. D., Wingfield, P. T., Lam, P. Y. S., Jadhav, P. K., Hodge, C. N., Domaille, P. J., & Chang, C. H. (1995) *Nat. Struct. Biol. 2*, 274−280.

Palmer, A. G., III, Rance, M., & Wright, P. E. (1991) *J. Am. Chem. Soc. 113*, 4371.

Peng, J. W., & Wagner, G. (1992) *Biochemistry 31*, 8571−8586.

Redfield, C., Boyd, J., Smith, L. J., Smith, R. A. G., & Dobson, C. M. (1992) *Biochemistry 31*, 10431−10437.

Rischel, C., Madsen, J. C., Andersen, K., & Poulsen, F. M. (1994) *Biochemistry 33*, 13997−14002.

Sacchettini, J. C., Gordon, J. I., & Banaszak, L. J. (1989) *J. Mol. Biol. 208*, 327−339.

Sacchettini, J. C., Scapin, G., Gopaul, D., & Gordon, J. I. (1992) *J. Biol. Chem. 267*, 23534−23545.

Scapin, G., Gordon, J. I., & Sacchettini, J. C. (1992) *J. Biol. Chem. 267*, 4253−4269.

Seale, J. W., Srinivasan, R., & Rose, G. D. (1994) *Protein Sci. 3*, 1741−1745.

Shaka, A. J., Keeler, J., Frenkiel, T., & Freeman, R. (1983) *J. Magn. Reson. 52*, 335−338.

Sklenar, V., Torchia, D. A., & Bax, A. (1987) *J. Magn. Reson. 73*, 375.

Wagner, G. (1995) *Nat. Struct. Biol. 2*, 255−257.

Wootan, M. G., Bernlohr, D. A., & Storch, J. (1993) *Biochemistry 32*, 8622−8627.

Yu, L., Zhu, C.-X., Tse-Dinh, Y.-K., & Fesik, S. W. (1996) *Biochemistry 35*, 9661−9666.

Zhang, O., Kay, L. E., Olivier, J. P., & Forman-Kay, J. D. (1994) *J. Biomol. NMR 4*, 845−858.


BI962018L